Veröffentlichung

Autoren

Müller, Lars;Kozulovic, Dragan;Radespiel, Rolf

Titel

Aerodynamic Performance of an Over-thewing Propeller Configuration at Increasing Mach Number

Publisher o. Konferenz

Proc. Deutscher Luft- und Raumfahrtkongress, Stuttgart, Germany

Jahr

2013

Internet-Link (Doi-Nr.)

AERODYNAMIC PERFORMANCE OF AN OVER-THE-WING PROPELLER CONFIGURATION AT INCREASING MACH NUMBER

L. Müller[1], D. Kožulović[1]*, R. Radespiel[2]

[1]Technische Universität Braunschweig, Institute of Jet Propulsion and Turbomachinery, Hermann-Blenk-Str. 37, 38108 Braunschweig

[2]Technische Universität Braunschweig, Institute of Fluid Mechanics, Hermann-Blenk-Str. 37, 38108 Braunschweig

Abstract

Over-the-wing propeller configurations show increased climb performance and, through effective acoustic shielding, reduced noise emissions when compared to a conventional tractor configuration. The main aerodynamic mechanisms could be identified by steady flow simulations of a simplified geometry and actuator disk. At takeoff, where the thrust coefficient is very high, the drag of the wing decreases much stronger than the thrust of the propeller. This paper investigates the cruise conditions where the thrust coefficient is by one order of magnitude lower. The numerical results give evidence that, at a moderate flight Mach number of 0.6, the beneficial influence of the over-the-wing propeller on the drag coefficient of the wing is negligibly small. On the other hand, the propeller loses an even larger relative amount of efficiency due to compressibility effects on the inflow velocity above the wing. As a result, the propulsive efficiency of a channel wing configuration is 16% smaller than the tractor value, increasing the fuel consumption by a similar percentage. Semi-empirical correlations show that, even at very low Mach numbers, a drawback of at least 5% remains. However, improvements concerning the propeller position and wing shape indicate a potential to restore two thirds of the performance loss.

Nomenclature

b, s	wing span, semispan
c	chord length
c_l, c_d	section lift, drag coefficients
c_p	pressure coefficient
C_D	drag coefficient
C_L	lift coefficient
C_T	thrust coefficient
Ma	Mach number
p,	static pressure
P_S	propeller shaft power
q,	dynamic pressure
Re	Reynolds number
S	wing area
T, t/t_{max}	thrust of one engine, relative local thrust
U, V, W	velocity components
x, y, z	Cartesian coordinates
y^+	dimensionless wall coordinate
α	angle of attack
η_P, η_{Pro}	propeller efficiency, overall propulsive efficiency
η_{PP}	propulsive efficiency of the propeller
ρ	density

Subscripts

0	propeller inflow (far upstream)
3	propeller slipstream (far downstream)
∞	free-stream
ref	reference (aircraft or cruise condition)
CW	channel wing
IW	isolated wing (clean wing)
TC	tractor configuration
g	geometric influence
t	influence of thrust

* Current affiliation: Hamburg University of Applied Sciences, Department of Automotive and Aeronautical Engineering, Berliner Tor 9, 20099 Hamburg.

1. INTRODUCTION

A considerable problem in Europe is the capacity shortage of the major hub airports [1]. The collaborate research centre SFB 880 (funded by Deutsche Forschungsgemeinschaft DFG) investigates the technologies for a commercial Cruise-Efficient Short Take-Off and Landing (CESTOL) aircraft which can operate from existing small airports in an air traffic network with more point-to-point connections. A reference configuration with turboprop engines in tractor configuration has been developed in an early stage of the research centre by using the Preliminary Aircraft Design and Optimization tool PrADO [2] (see layout in Fig. 1). At similar cruise performance and direct operating costs (DOC) as a state-of-the-art transport aircraft with passive high-lift devices, it can operate from 800 metre-long runways [3].

This paper is based on the results of a sub-project in the SFB 880 framework that focuses on over-the-wing propeller integration at the CESTOL aircraft. A major advantage of such an arrangement is considered to be its noise shielding capability which was confirmed by aeroacoustic simulations. At takeoff, the sound pressure level at the ground could be reduced by 6 dB compared to a conventional tractor configuration [4] which is of particular importance considering the open rotor noise issue.

Moreover, it was shown for the takeoff configuration with internally blown flaps that such an arrangement reaches a 2-3% higher climb angle than a conventional tractor design [4][5]. Furthermore, embedding the propeller into a channel wing is beneficial to minimize the nose-down pitching moment due to thrust. The computational fluid dynamics (CFD) results reveal that the close integration leads to a trade-off between propeller and wing performance. While the propeller loses 20% of its efficiency due to a considerably higher inflow velocity above the suction side, the wing achieves twice the lift-to-drag ratio. At takeoff, where the thrust is high and the free-stream dynamic pressure is small, the positive effect on the drag of the wing is considerably larger than the loss in thrust which is why a higher propulsive efficiency can be achieved.

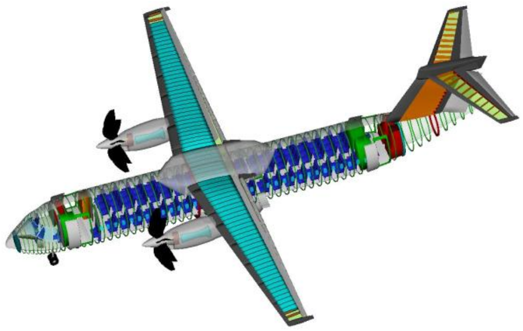

FIGURE 1. Baseline design of CESTOL aircraft.

This paper extends the investigation to cruise conditions where the thrust coefficient is by one order of magnitude smaller. It is therefore assumed that the influence of the propeller on the pressure distribution with its drag reduction effect is significantly decreased. A crucial factor is whether the propeller still loses a similar amount of its efficiency due to the inflow conditions above the wing. Johnson [6] showed that the propeller efficiency may even increase by over-the-wing installation.

As done in previous work, simplified wing and actuator disk geometries were used to compare the channel wing with a reference tractor configuration. Reynolds-averaged Navier-Stokes (RANS) simulations have been conducted at three different Mach numbers (0.4, 0.5 and 0.6) to quantify the above-mentioned effects and to find a correlation between cruising speed, inflow velocity to the propeller and propulsive efficiency of the aircraft.

2. TEST CASE

2.1. Flow Conditions

The key parameters of the STOL aircraft at cruise conditions, as determined in the preliminary design process, are specified in Table 1. At similar atmospheric conditions with a density of ρ_∞ = 0.384 kg/m³ and a temperature of 219 K, different lift and thrust coefficients and a lower Mach number were used in this fundamental study.

	STOL Aircraft	CFD test case
Flight altitude	10600 m	
Flight Mach number	0.74	0.6
Wing area	92 m²	67.3 m²
Lift coefficient C_L	0.458	0.555
Drag coefficient C_D	0.0316	
Thrust coefficient C_T	0.0316	0.05

TAB 1. Specifications of the cruise conditions.

As the reference aircraft has a local lift coefficient of c_l = 0.555 at the spanwise position of the propeller, this value was used as C_L for all numerical flow simulations. A reference cruise Mach number of 0.6 and a corresponding thrust coefficient of C_T = 0.05 were selected as the actuator disk model cannot deal with supersonic inflow velocities that occur locally above $Ma_\infty \approx 0.63$. However, computations at two lower Mach numbers (0.4 and 0.5) have been conducted to quantify the influence of cruising speed on aerodynamic performance. For the profile section at the propeller (chord length of c = 3.67 m) and a flight velocity of U_∞ = 178 m/s (Ma_∞ = 0.6), the flow is characterized by a Reynolds number of Re = $17.5 \cdot 10^6$ which is similar to the takeoff case.

2.2. Configurations and Geometry

In this paper, a channel wing with partially embedded over-the-wing propeller is compared to a conventional tractor configuration which was designed as a reference (cf. Fig. 2). The embedding depth, clearance and axial propeller position of the channel wing were identical to the takeoff configuration as investigated in [7].

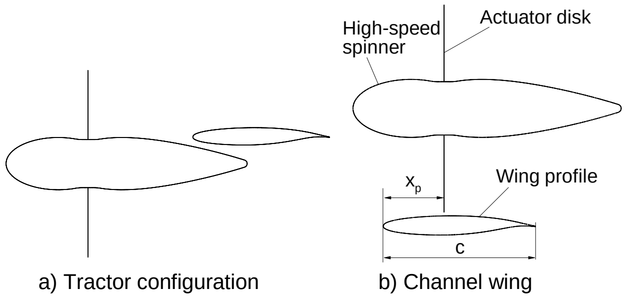

FIGURE 2. Side view of CFD geometry with chord length c and axial propeller position x_P.

The geometry, aerodynamic requirements and boundary conditions of all test cases are based on the preliminary design of the STOL aircraft. For this basic research work, a simplified test case with an untwisted, rectangular wing (wingspan b = 5 c) and a propeller with generic nacelle was designed. In order to exclude aspect ratio dependencies and tip vortices, a symmetry condition was applied at both ends of the wing segment. For the constant profile along the span, the transonic DLR-F15 airfoil [8] with a maximum thickness of 12.6% was selected.

The turboprop engine was simulated by using an actuator disk and a generic, axisymmetric nacelle with ellipsoidal high-speed spinner. The propeller disk has a diameter of D_P = 5 m = $1.36 \cdot c$ and a hub ratio of 0.258. The design parameters of the nine-blade high-speed propeller, including the aerodynamic characteristics, were taken from a similar project [9].

3. NUMERICAL SETUP

3.1. Grid Generation

A cylindrical computational domain with a diameter of 20 chord lengths (cf. Fig. 3) was selected to apply a symmetry condition on the side walls (Fig. 4). As the influence of laminar boundary layers on the aerodynamic properties was assumed to be negligibly small at cruise conditions, all wing and nacelle surfaces were assigned a turbulent viscous wall condition. The unstructured grids were created with the commercial grid generator *Centaursoft Centaur* and contain approximately 10 million nodes. Grid sensitivity studies with three different sizes were performed for the 2D airfoil to reveal mesh size dependencies. Aiming at a dimensionless wall distance of the first cell of y^+ = 1, a reasonable grid resolution was determined. In order to further improve the accuracy of the 3D solution, regions of expected high gradients like propeller slipstream, wake and possible shock regions above the wing were refined by using grid sources, see Fig. 5.

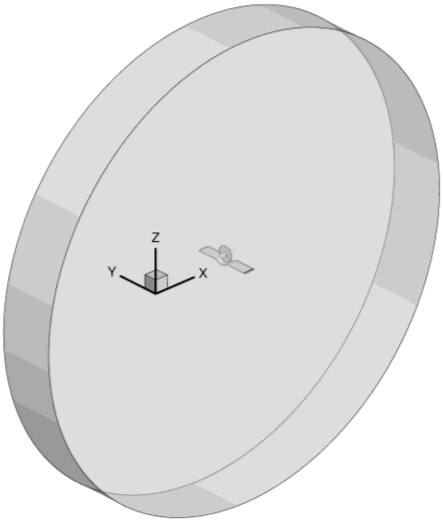

FIGURE 3. Geometry of the computational domain.

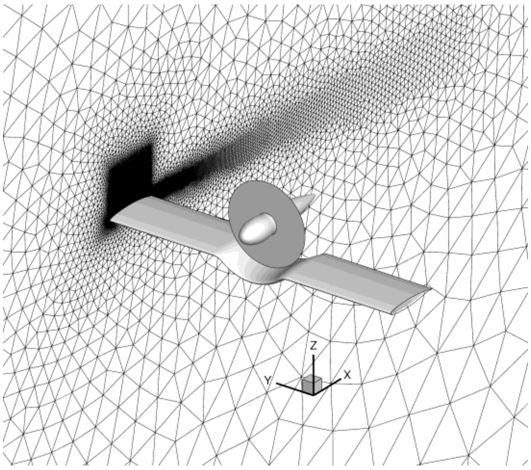

FIGURE 4. Detail of channel wing CFD geometry.

3.2. Numerical Method

The steady CFD simulations were conducted by using the DLR TAU code [10] for solving the RANS equations on the unstructured grids. Turbulence was modelled by the Spalart-Allmaras one-equation formulation [11]. The inviscid fluxes of the Navier-Stokes-Equations and the convective fluxes of the turbulence equations were discretized by a second order upwind scheme. On the other hand, all viscous fluxes were discretized by a central scheme using a full gradient approach. A backward Euler relaxation solver was chosen to enable an implicit time integration scheme. Using a CFL number of 5, convergence was usually achieved after 30000 iterations.

3.3. Actuator Disk

The active actuator disk model uses blade element theory to calculate the steady forces applied to the fluid [12]. This means that the actual inflow is taken into account which is particularly important for installed propellers. According to the propeller design [9], the distributions of blade twist and chord length as well as the aerodynamic characteristics were prescribed at discrete radii. The resulting torque leads to a realistic swirl in the propeller slipstream which may interact with the wing.

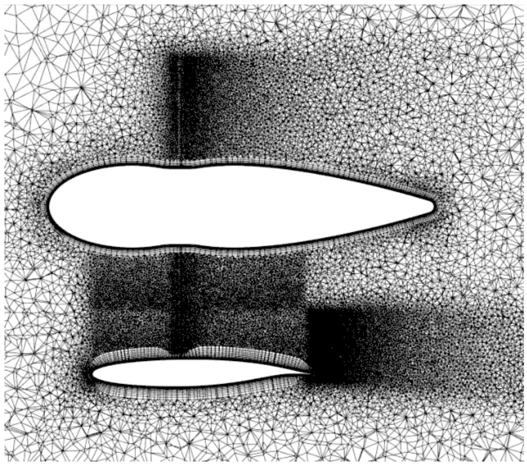

FIGURE 5. Midspan cross section of 3D channel wing mesh showing source-based refinements.

4. RESULTS

As shown for takeoff conditions [5][7], the propeller installation effects of both tractor and over-the-wing configurations arise from a mutual influence between the propeller and wing. Because the aerodynamic mechanisms for these two parts of the aircraft are quite different, they will be discussed separately in Sec. 4.1 and 4.2. To furthermore assess the performance of the entire configurations, an evaluation of the overall thrust and drag forces is eventually provided in Sec. 4.3. The propulsive efficiency is considered an appropriate figure of merit for cruise conditions. Taking the cruise Mach number into account, some design requirements can be derived for the channel wing which is compared to the tractor configuration.

4.1. Wing Aerodynamics

4.1.1. Installation Effects at Cruise Conditions

Before analysing the influence of the actual flight Mach number on the aerodynamic characteristics, the general installation effects will be discussed for a constant Mach number 0.6.

The flow field around the clean wing profile at cruise conditions (Fig. 6) is obviously different from that at takeoff where the blown Coanda flap is deployed at 45° [7]. Instead of two suction peaks, there is only one near the leading edge. However, the high velocity region above the suction side reaches from the leading to the trailing edge with its maximum values and extension right in the plane of the over-the-wing propeller (x_P/c = 0.4). Hence, this kind of engine position has the highest average inflow velocity and strongest vertical gradient in the whole flow field. In contrast, the tractor position leads to a relatively homogeneous inflow at a velocity that is slightly below the freestream value. Fig. 7 and 8 show the altered flow field with installed engine. Due to the stagnation effect of the nacelle, the flow velocity rises in a small distance to the propeller disk with a local maximum on the convex surface of the spinner. It further increases in the slipstream of the propeller where, as seen for the tractor configuration, the Mach number level around the wing is changed. However, even higher Mach numbers can be observed above the channel wing where the entire slipstream affects the upper surface. In addition, the suction peaks of the nacelle and spinner are added to the flow field at this particular position. It can be easily seen that the velocity level, at which the propeller operates, is much higher for the over-wing installation. As also evident from Fig. 9, the high Mach numbers at this configuration lead to high negative pressure coefficients on the wing which may reach the critical value at larger cruising speeds.

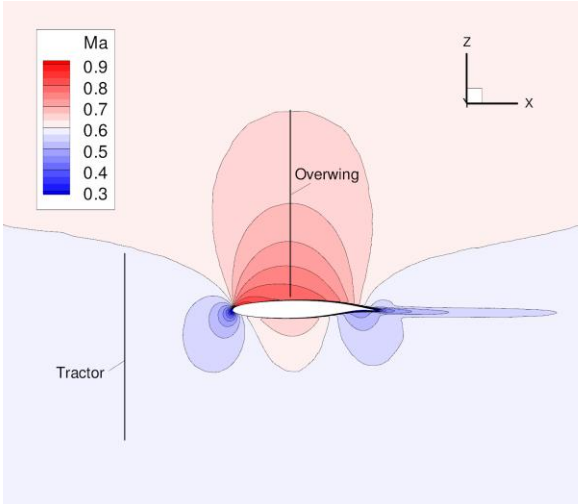

FIGURE 6. Mach number distribution around clean wing. Possible propeller positions are indicated.

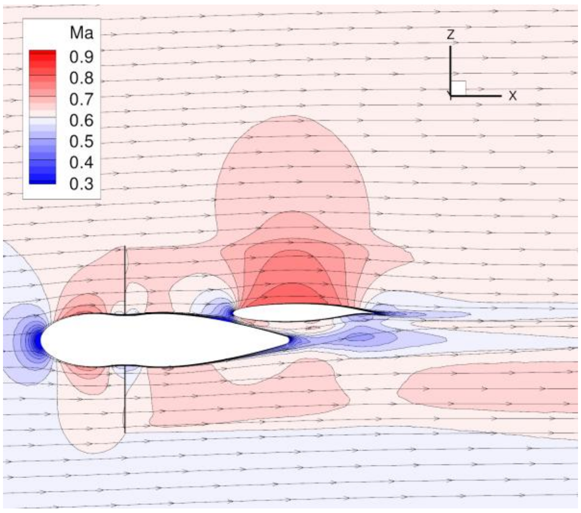

FIGURE 7. Midspan flow field of tractor configuration.

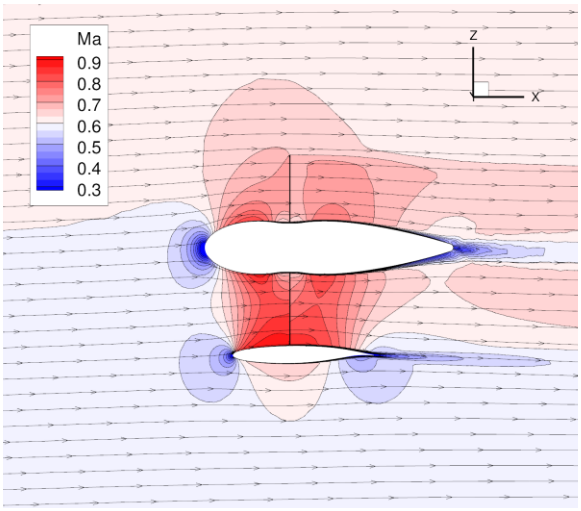

FIGURE 8. Midspan flow field of channel wing.

The chordwise pressure distribution of the tractor is shown in Fig. 9 at two characteristic positions in the propeller slipstream (y/s = 0.2 and -0.2). The reason is that the local lift coefficient is minimum or, respectively, maximum at these coordinates (cf. Fig. 10). As the spanwise lift distribution of the channel wing is almost symmetric, only the pressure coefficient at the midspan section, where c_l has its highest value, is shown in Fig. 9. Despite varying positions, some clear differences between tractor and channel wing can be observed. While the tractor at y/s = -0.2 has a distinct suction peak at the leading edge, this feature is missing at the channel wing where the additional suction pressure is distributed over the upper surface with a plateau upstream of the propeller. This kind of long suction peak is already known from the takeoff case where it is responsible for a strong reduction of the pressure drag [7].

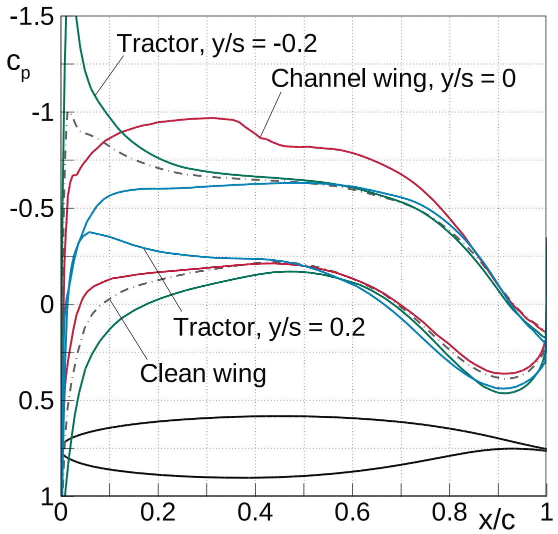

FIGURE 9. Pressure distributions at $Ma_\infty = 0.6$.

Figures 10 and 11 show the spanwise (three-dimensional) effects of propeller installation at cruise. Significant differences between tractor and channel wing are evident for the c_l distributions (Fig. 10). As mentioned before, the overall lift coefficient was adjusted to a constant value of C_L = 0.555 for all configurations. It is well known that the swirl in the slipstream of a tractor propeller leads to up- and downwash regions at the wing and, accordingly, a sinusoidal lift distribution behind the propeller [13][14]. This effect is completely missing at the over-the-wing configuration as the slipstream does not impinge on the leading edge. As the shape of the c_l curve is, in contrast to the tractor, comparable to that at takeoff [7], wing twist may be applied to equalize the spanwise lift distribution and thus lowering induced drag.

The spanwise drag distribution (Fig. 11) reveals that the c_d level of the channel wing is generally below the magnitudes of the tractor configuration. However, the difference is much smaller compared to takeoff conditions where the combination of high thrust and deflected flap led to large drag increments at the tractor. At cruise, the drag is just redistributed along the span according to the local flow angle rather than increased in the slipstream. The channel wing distribution, on the other hand, has a similar shape as at takeoff. Only the local maximum at midspan is relatively larger and now surpasses the clean wing.

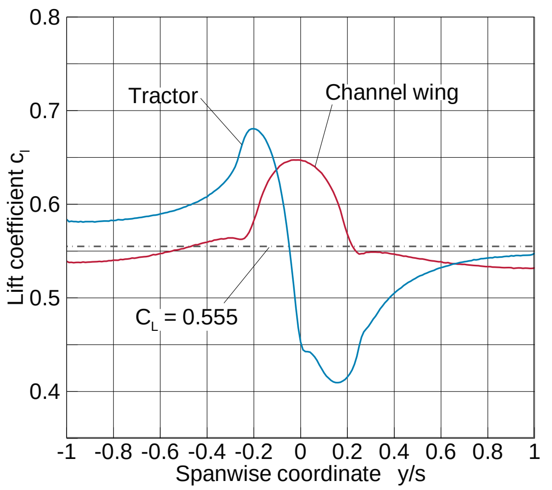

FIGURE 10. Spanwise lift coefficient at Ma∞ = 0.6.

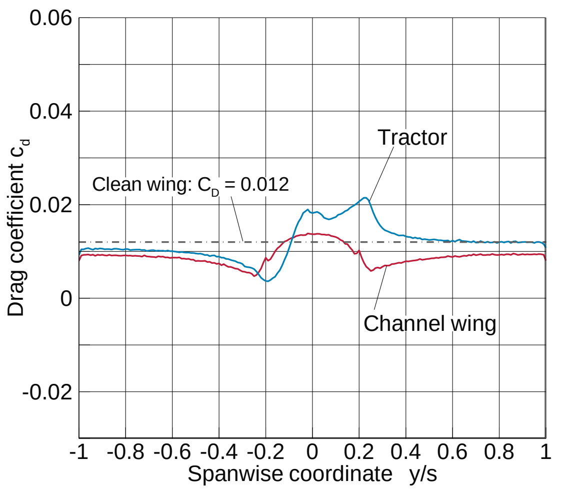

FIGURE 11. Spanwise drag coefficient at Ma∞ = 0.6.

4.1.2. Mach Number Dependency

To understand the impact of propeller integration on the performance of a channel wing, one must keep in mind the importance of ratio between thrust and dynamic pressure or, respectively, the thrust coefficient

$$C_T = \frac{2T}{S \cdot q_\infty} \tag{1}$$

It has been shown that, at least for high thrust coefficients of about 0.3 at takeoff, beneficial effects on the wing lead to enhanced overall performance [7].

The following results show the differences between tractor and channel wing aerodynamics with increasing Mach number from Ma∞ = 0.4 to 0.6. More specifically, only the Mach number has been varied in the numerical simulations while the free-stream density and the thrust remained constant. This enables aerodynamic investigations of Ma∞ and C_T dependencies as thrust coefficient and dynamic pressure change accordingly. However, in this paper only the Mach number influence for a constant C_T shall be discussed. Together with a constant lift coefficient C_L, this case applies to an aircraft cruising in straight and level flight ($C_L = W/(q_\infty S)$, $C_T = C_D$) at a certain (usually the optimum) lift-to-drag ratio C_L/C_D.

A thrust coefficient of C_T = 0.05 has been selected for this study as it is valid for the reference cruise conditions with a corresponding Mach number of 0.6. This means that the results at the two other velocities (Ma∞ = 0.4 to 0.5) had to be transferred to the above-mentioned reference thrust coefficient. At a constant lift coefficient, the influence of propeller installation on the aerodynamic performance of the wing is fully captured by the drag coefficient difference to the isolated wing (subscript *IW*). Simulations of the tractor and channel wing configurations with zero thrust have been conducted to split this difference into an increment due to geometry (subscript *g*) and another due to thrust (subscript *t*):

$$\Delta C_D = C_D - C_{D,IW} = \Delta C_{D,g} + \Delta C_{D,t} \tag{2}$$

The geometrically caused $\Delta C_{D,g}$ can be explained by the influence of the nacelle (for both configurations) and the larger wetted surface of the channel wing. It is obtained from the simulations with deactivated thrust:

$$\Delta C_{D,g} = C_{D,T=0} - C_{D,IW} = f_g(\mathrm{Ma}_\infty) \tag{3}$$

On the other hand, the pure thrust effect is determined by the difference between the actual configuration with and without thrust:

$$\Delta C_{D,t} = C_{D,T=const} - C_{D,T=0} \tag{4}$$

This increment is proportional to the thrust coefficient if we assume that the induced drag force depends on the thrust:

$$\Delta D_t = T \cdot f_1(\mathrm{Ma}_\infty) \tag{5}$$

$$\Delta C_{D,t} = \frac{\Delta D_t}{S \cdot q_\infty} = \frac{T \cdot f_1(\mathrm{Ma})}{S \cdot q_\infty} = C_T \cdot f_2(\mathrm{Ma}_\infty) \tag{6}$$

It is obvious that the thrust coefficient must be constant to extract the Mach number dependency $f(\mathrm{Ma}_\infty)$. As mentioned above, the drag increments $\Delta C_{D,t}$ were converted under consideration of a constant (reference) thrust coefficient $C_{T,ref}$ = 0.05.

$$\Delta C_{D,t} = C_T \cdot f_2(\mathrm{Ma}_\infty) = \frac{C_T}{C_{T,ref}} C_{T,ref} \cdot f_2(\mathrm{Ma}_\infty)$$

$$\Leftrightarrow \Delta C_{D,t} \frac{C_{T,ref}}{C_T} = const \cdot f_2(\mathrm{Ma}_\infty)$$

$$\Leftrightarrow \Delta C_{D,t,C_T=const.} = \Delta C_{D,t} \frac{q_\infty}{q_{\infty,ref}} = f_t(\mathrm{Ma}_\infty) \tag{7}$$

Hence, the thrust-induced drag coefficients of the computations with Ma∞ = 0.4 and 0.5 have been multiplied with the ratio of the actual dynamic pressure and the reference value from a flight velocity of Ma∞ = 0.6. Furthermore, as the reference aircraft has two engines and a wing area that is 1.37 times larger than that of the simulated wing segment, all values were scaled by a factor of 2/1.37 = 1.46.

The resulting drag increments of the tractor configuration (subscript *TC*) and channel wing (subscript *CW*) are shown as symbols in Fig. 12. In addition, the difference in drag coefficient between these two configurations is indicated:

$$\Delta C_{D,CW-TC} = \Delta C_{D,CW} - \Delta C_{D,TC}\ . \tag{8}$$

It is evident that the channel wing at all three Mach numbers has a lower drag as the tractor configuration. However, the difference is significantly reduced when the Mach number is increased. The question arises whether the drag will exceed the level of the tractor at Mach numbers above 0.6. For this reason, a semi-empirical correlation, which is based on theoretical considerations (Eq. (5)) and calibrated with numerical data, was developed.

Based on Eq. (7), the correlation of (corrected) drag increment and Mach number, $f_t(\mathrm{Ma}_\infty)$, was determined using the three data points of the CFD simulation for a least squares regression. The only assumption was that the functions $f_g(\mathrm{Ma}_\infty)$ and $f_t(\mathrm{Ma}_\infty)$ must either strictly monotonically increase or decrease following a power law:

(9) $$f_{g,t} = C_1 \cdot \mathrm{Ma}_\infty^n + C_2$$

All obtained constants for the corresponding parts of the drag difference are specified in Table 2. It is obvious just from the constants that the channel wing, compared to the tractor, has a higher drag penalty through its larger wetted surface and nacelle position but also a significantly larger benefit through propeller integration (at moderate Ma_∞).

	n	C_1	C_2
$\Delta C_{D,g,TC}$	1	-0.0014	0.00270
$\Delta C_{D,g,CW}$	1	-0.0006	0.00390
$\Delta C_{D,t,TC}$	4	0.0102	-0.00065
$\Delta C_{D,t,CW}$	6	0.0484	-0.00457

TAB 2. Coefficients for the drag correlation.

This behaviour is also reflected in the continuous curves in Fig. 12 which are based on Eqs. (3), (7) and (9). The overall difference between channel wing and tractor is obtained by inserting the individual functions in Eq. (8). It is then evident from the orange curve that the channel wing has the largest advantage at low speed where the drag increment is almost independent of the flight Mach number. Between Ma_∞ = 0.4 and 0.5, however, a sudden drag increase leads to the result that the drag of the tractor configuration is reached ($\Delta C_{D,CW\text{-}TC}$ = 0) at a certain cruising speed ($\mathrm{Ma}_\infty \approx 0.66$).

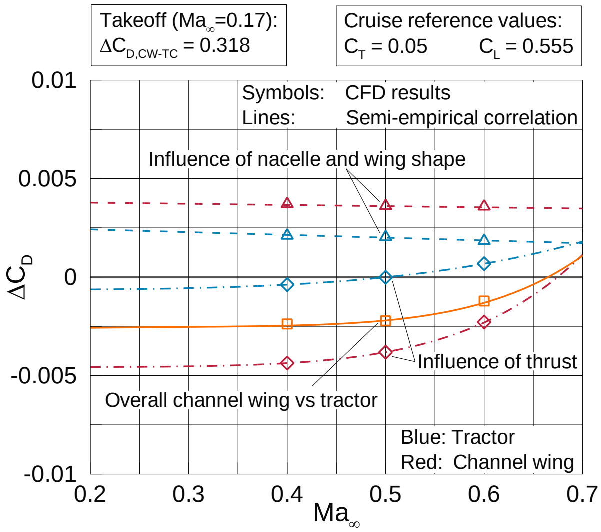

FIGURE 12. Drag coefficient increments depending on cruising speed.

4.2. Propeller Aerodynamics

It has been already shown in [3] that an over-the-wing propeller at takeoff loses a significant amount of efficiency due to an increased inflow velocity and an inhomogeneous thrust distribution. The latter effect which arises from a strong vertical gradient in the velocity field above the wing, is also present at cruise conditions, cf. Fig. 13. Although the flap is now retracted, a similar relative distribution is found where almost no thrust is generated near the wing surface. In addition, a lateral shift of thrust due to the positive angle of attack (takeoff: α = 0 deg) is found at cruise.

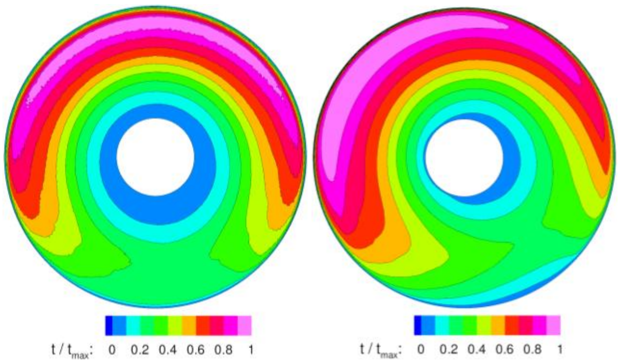

(a) Takeoff conditions, $C_T = 0.675$

(b) Cruise conditions, $C_T = 0.05$

FIGURE 13. Distributions of relative thrust t/t_{max} on actuator disk.

It is however assumed that the major part of the loss in propeller efficiency is due to the additional inflow velocity that is present at the over-the-wing position. This effect shall be estimated by simple momentum theory in the following way. First, the propulsive efficiency of the propeller is defined as the ratio between the propulsion power and the power added to the fluid:

(10) $$\eta_{PP} = \frac{T \cdot U_\infty}{\frac{\dot{m}}{2}(U_3^2 - U_0^2)},$$

where U_0 is the inflow velocity and U_3 is the slipstream velocity far downstream of the propeller. Using the definition of the thrust

(11) $$T = \dot{m}(U_3 - U_0)$$

yields:

(12) $$\eta_{PP} = \frac{2U_\infty}{U_0 + U_3}.$$

The unknown velocity U_3 can be determined if the mass flow in Eq. (11) is substituted by its definition in the propeller plane with a local velocity of $U_P = \frac{1}{2}(U_0 + U_3)$ and A_P as the area of the propeller disk:

(13) $$\dot{m} = \frac{\rho}{2}(U_0 + U_3)A_P$$

$$T = \dot{m}(U_3 - U_0) = \frac{\rho}{2}A_P(U_0 + U_\infty)(U_3 - U_0)$$

$$\Leftrightarrow \frac{2T}{\rho A_P} = U_3^2 - U_0^2$$

(14) $$\Leftrightarrow U_3 = \pm\sqrt{\frac{2T}{\rho A_P} + U_0^2}$$

where only the positive solution makes physically sense. The propulsive efficiency of an over-the-wing propeller relative to a tractor configuration then reads:

(15) $$\frac{\eta_{PP}}{\eta_{PP,TC}} = \frac{U_{0,TC} + U_{3,TC}}{U_0 + U_3} = \frac{U_{0,TC} + \sqrt{\frac{2\,T}{\rho A_P} + U_{0,TC}^2}}{U_0 + \sqrt{\frac{2\,T}{\rho A_P} + U_0^2}}$$

It is worth mentioning that the disk loading (or thrust density) T/A_P is small for high efficiency propellers. An approximation can be made for large inflow velocities U_0 where the comparatively small term $\frac{2}{\rho}\frac{T}{A_P}$ can be neglected:

$$\frac{\eta_{PP}}{\eta_{PP,TC}} \approx \frac{U_{0,TC}}{U_0} \approx \frac{U_\infty}{U_\infty + \Delta U}$$

As the same propeller is used for all configurations, the ratio of propulsive efficiencies can be approximately replaced by the ratio of propeller efficiencies $\eta_P/\eta_{P,TC}$. Furthermore, the velocities shall be expressed by the Mach numbers:

(16) $$\frac{\eta_P}{\eta_{P,TC}} = \frac{1}{1+\frac{\Delta \mathrm{Ma}}{\mathrm{Ma}_\infty}}$$

To get the function of the relative propeller efficiency depending on the cruising speed one only has to find a correlation between the relative additional inflow Mach number ΔMa/Ma$_\infty$ and flight Mach number Ma$_\infty$.

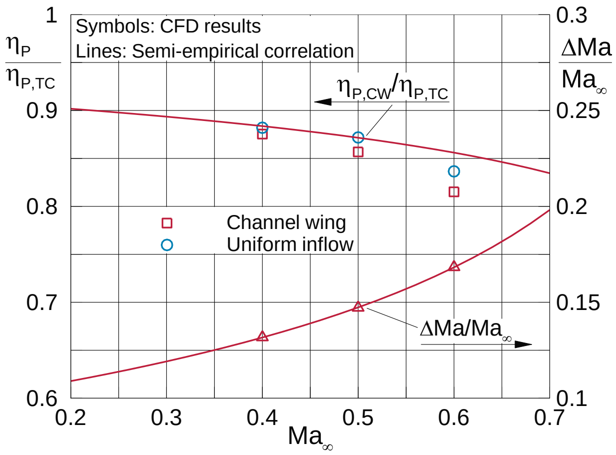

FIGURE 14. Relative propeller efficiency and relative inflow velocity dependent on cruising speed.

First, it can be assumed that ΔMa/Ma$_\infty$ will somehow increase with Ma$_\infty$ due to compressibility effects. From a potential theory point of view, the velocity increment ΔMa that is induced by the wing is directly connected to the pressure coefficient at that position:

(17) $$c_p = -2\frac{\Delta \mathrm{Ma}}{\mathrm{Ma}_\infty}$$

Thus, the growth of ΔMa/Ma$_\infty$ can be approximated by the factor of the *Prandtl-Glauert-Rule*

(18) $$\frac{1}{\sqrt{1-Ma_\infty^2}}$$

which is valid for the pressure coefficient. However, another complex dependency exists due to the varying α at constant C_L. To find an empirical correlation, numerical simulations of the channel wing with zero thrust have been conducted. It was thus possible to extract the average inflow velocity increments at the disk for the three considered Mach numbers, see delta-shaped symbols in Fig. 14. By dividing the obtained values of ΔMa/Ma$_\infty$ by the compressibility factor (Eq. (18)), a linear function was evident:

(19) $$\frac{\Delta \mathrm{Ma}}{\mathrm{Ma}_\infty} = (C_3 \cdot Ma_\infty + C_4)\frac{1}{\sqrt{1-Ma_\infty^2}}$$

The two constants could be determined by a least squares regression of the CFD data points (C_3 = 0.0696, C_4 = 0.0928). This means that the additional inflow velocity at the channel wing propeller has an initial value of about ΔMa/Ma$_\infty$ ≈ 0.1 and increases disproportionately with the cruising speed, see Fig. 14.

Inserting Eq. (19) in Eq. (16) leads to the semi-empirical correlation between the relative propeller efficiency and the flight Mach number. As seen in Fig. 14, an increasing amount of η_P is lost when flying faster. The CFD simulations provided the absolute propeller efficiency for both configurations

(20) $$\eta_P = \frac{T \cdot U_\infty}{P_S}$$

As the desired ratio between channel wing and tractor

(21) $$\frac{\eta_P}{\eta_{P,TC}} = \frac{P_{S,TC}}{P_S}$$

is independent of the thrust coefficient and dynamic pressure, no correction for $C_{T,ref}$ = 0.05, as done for the drag correlation, was necessary. Figure 14 shows the numerically obtained relative propeller efficiencies as square symbols. The deviation to the expected values on the curve is mainly caused by the loss due to inhomogeneous thrust distribution as some blade positions lead to unfavourable angles of attack [3]. To extract this effect and to validate the correlation, numerical simulations of the isolated propeller at accordingly increased inflow Mach number Ma$_0$ = Ma$_\infty$ + ΔMa have been conducted (see Fig. 14, blue circles). While the results for the two lower Mach numbers are in good agreement with the curve, there is a significant difference for Ma$_\infty$ = 0.6. The reason is that an equal figure of merit was assumed for both tractor and over-the-wing propellers, cf. Eq. (16). This is apparently not valid at high inflow velocities above the flight speed the propeller was designed for (channel wing: Ma$_0$ = 0.7 at Ma$_\infty$ = 0.6).

4.3. Overall Performance

Having discussed the wing and propeller performance of a channel wing at increasing Mach number in the previous two sections, the overall configuration shall be assessed in the following.

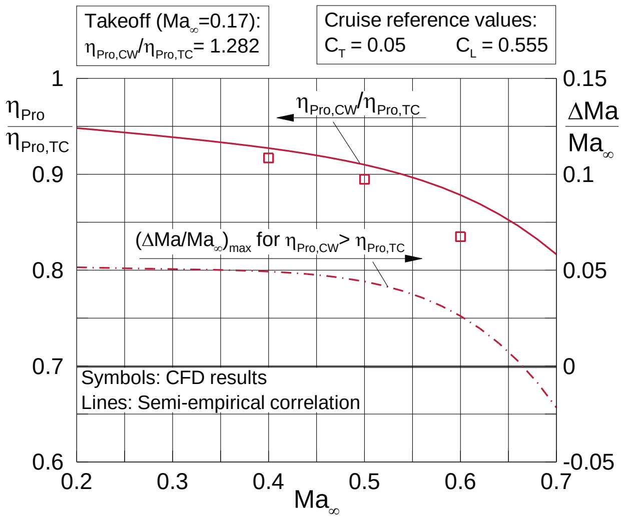

FIGURE 15. Relative propulsive efficiency and maximum allowed inflow velocity increment dependent on cruising speed.

Considering the axial force balance by subtracting the drag increment $\Delta D = \Delta C_D q_\infty S_{ref}$ from the total thrust (2 engines), the propulsive efficiency of the aircraft is:

(22) $$\eta_{Pro} = \frac{(2T-\Delta D)U_\infty}{2P_S} = \frac{TU_\infty}{P_S} - \frac{\Delta DU_\infty}{2P_S}$$

Using Eq. (20) to substitute the shaft power P_S and inserting the definition of ΔD, Eq. (22) reduces to

$$\eta_{Pro} = \eta_P\left(1 - \frac{\Delta C_D q_\infty S_{ref}}{2T}\right)$$

or, respectively, relative to the tractor

(23) $$\frac{\eta_{Pro}}{\eta_{Pro,TC}} = \frac{\eta_P}{\eta_{P,TC}}\left(1 - \frac{\Delta C_D}{C_T}\right)$$

where $\eta_P/\eta_{P,TC}$ (Eqs. (16), (19)) and ΔC_D (Eq. (8)) can be inserted. The resulting correlation for $C_T = C_{T,ref} = 0.05$ is shown in Fig. 15 together with the data points from the simulations. As the wing drag increases and the propeller efficiency decreases with increasing Mach number, it is not surprising that the overall propulsive efficiency of the channel wing also decreases. It is, however, noticeable that even at a very low Mach number of 0.2 the efficiency of the tractor configuration cannot be reached.

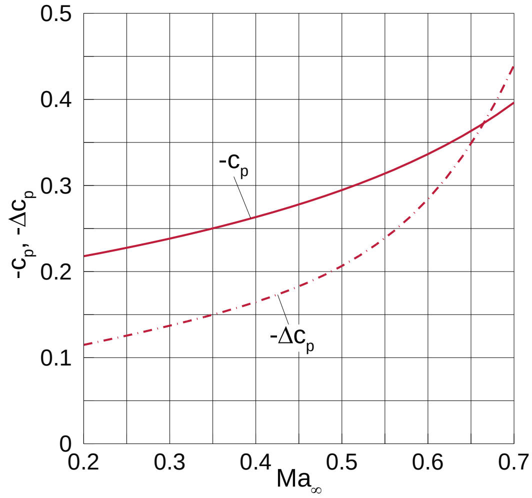

FIGURE 16. Average pressure coefficient at the propeller position in the flow field of the clean wing.

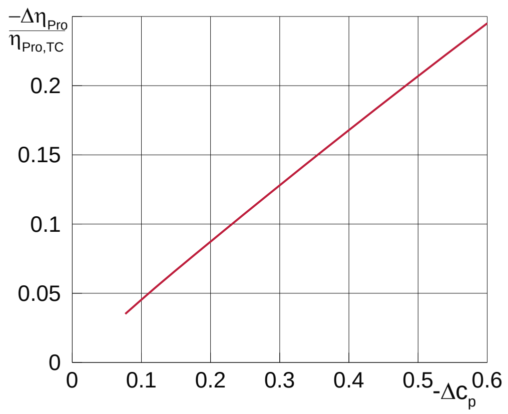

FIGURE 17. Loss of overall efficiency due to low pressure coefficient above the wing.

The question arises what conditions are necessary to enable equal performance. Looking at Eqs. (23) and (16) it is obvious that channel wing design has to aim at a reduction of the inflow velocity to the propeller. Using the above-mentioned equations and setting $\eta_{Pro}/\eta_{Pro,TC} = 1$, one obtains a correlation between the maximum allowed velocity increment at the propeller position and the flight Mach number:

(24) $$\left(\frac{\Delta \mathrm{Ma}}{\mathrm{Ma}_\infty}\right)_{max} = -\frac{\Delta C_D}{C_T}$$

The right-hand side can be interpreted as figure of merit for over-the-wing installations. As seen in Fig. 15 for the channel wing geometry considered in this investigation, no additional inflow velocity is allowed for Mach numbers lager than 0.66. Based on Eqs. (17) and (19), Fig. 16 shows the average pressure coefficient at the actuator disk position above the wing together with the difference to the allowed value for $\eta_{Pro}/\eta_{Pro,TC} = 1$. This means that the local pressure coefficient on the suction surface of the wing is approximately by 0.12 too low at $\mathrm{Ma}_\infty = 0.4$ and by 0.38 too low at $\mathrm{Ma}_\infty = 0.7$. The loss of propulsive efficiency dependent on the c_p increment is provided by Fig. 17. As an almost linear function is evident, each deviation of $-\Delta c_p = 0.1$ from the allowed local pressure coefficient costs more than 4% of overall efficiency.

4.4. Influence of Design Parameters

At fixed thrust, two variables must be considered in channel wing design to enhance the efficiency (cf. Eq. (24)):

- The effectiveness of over-the-wing propeller installation on the drag reduction $\Delta C_D/C_T$.
- The inflow velocity to the propeller $\Delta\mathrm{Ma}/\mathrm{Ma}_\infty$.

These issues are connected to the following design parameters:

- The position of the propeller in the wing flow field.
- The pressure distribution of the clean wing.

It is expected that each design parameter has influence on both variables ($\Delta C_D/C_T$, $\Delta\mathrm{Ma}/\mathrm{Ma}_\infty$). The first-mentioned parameter was investigated through a variation of the axial propeller position x_P/c. Between the leading edge and trailing edge, six equidistant positions have been considered at a Mach number of $\mathrm{Ma}_\infty = 0.6$.

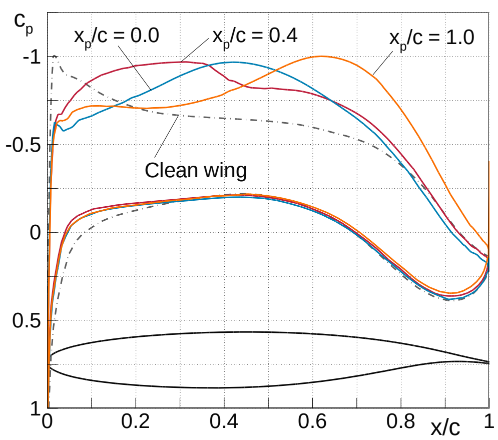

FIGURE 18. Pressure distributions at midspan ($y/s = 0$) for various axial propeller positions at $\mathrm{Ma}_\infty = 0.6$.

The pressure distributions for the extreme propeller positions, including the reference $x_P/c = 0.4$, are shown in Fig. 18. It is obvious that the completely different distributions on the suction surface will lead to different drag coefficients. Having the local surface orientation in mind, a front-loaded distribution, as evident for the reference position, is advantageous.

As seen in Fig. 19, the local optimum regarding ΔC_D is indeed at mid-chord. Unfortunately, this is an unfavourable location for the propeller as its efficiency has the lowest value here. Better positions can be found right at the leading edge and trailing edge with an optimum at the latter one. As these two opposing trends contribute to the overall efficiency, $\eta_{Pro}/\eta_{Pro,TC}$ shows only little variation with the chordwise position. However, the best performance is achieved by a propeller at the trailing edge.

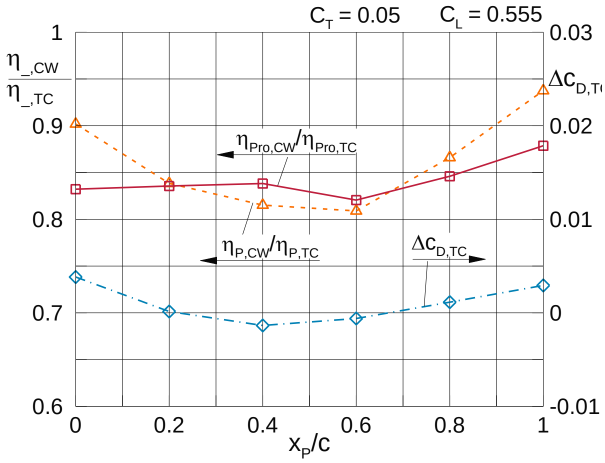

FIGURE 19. Effect of propeller position on drag, propeller efficiency and overall efficiency.

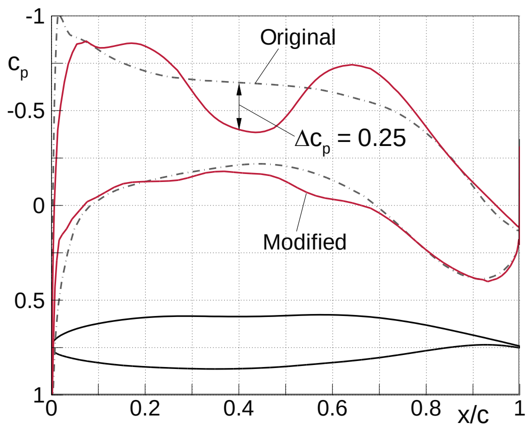

FIGURE 20. Midspan pressure distribution of modified profile.

	α_{cruise} [°]	L/D_{cruise}
Original DLR-F15 profile	1,4	48,3
Modified profile	0,7	49,3

TAB 3. Aerodynamic figure of merit of modified profile.

As second parameter, the pressure distribution of the clean wing was adapted to the needs of the propeller. More specifically, an attempt was made to increase the pressure coefficient below the actuator disk in order to lower its inflow velocity. By changing the curvature distribution of the camber line together with a 10% reduction of the maximum thickness it was possible to increase the local c_p by 0.25, see Fig. 20. Despite this radical measure, the modified profile reaches the lift-to-drag ratio of the original geometry (cf. Table 3), at least for Ma_∞ = 0.6 (which is below the design Mach number of the DLR-F15 airfoil). Based on Figs. 17, 19 and 20 one can roughly estimate the potentials of optimizing airfoil and propeller positions. This potential appears as an increase of 10% in propulsive efficiency. This improvement does not render the channel wing equally efficient as the tractor at Ma=0.6, but now the remaining difference is in the order of 5%.

5. CONCLUSIONS AND OUTLOOK

A generic channel wing, consisting of a rectangular wing segment and an over-the-wing propeller was investigated at cruise conditions regarding the aerodynamic performance compared to a conventional tractor configuration. RANS simulations have been conducted at three Mach numbers (0.4, 0.5 and 0.6) to quantify the mutual influence of wing and propeller. Based on the results of the CFD simulations at constant thrust and lift coefficient, semi-empirical correlations between the drag increment on the wing ΔC_D as well as the relative propeller efficiency $\eta_P/\eta_{P,TC}$, and the flight Mach number Ma_∞ could be developed. Some approximations were feasible by taking the tractor configuration as a reference while the remaining constants were determined by a least squares regression of the numerical data. The Mach number dependencies can be summarized as follows:

- Like for takeoff conditions, an over-the-wing propeller decreases the drag of the wing at moderate cruise Mach numbers.
- Above a certain flight velocity, a channel wing produces more drag than a tractor configuration due to the unfavourable location of the nacelle and a larger wetted surface.
- The propeller efficiency continuously declines with Ma_∞ as the local inflow velocity or relative additional Mach number $\Delta Ma/Ma_\infty$, respectively, increases.
- As a result, the overall propulsive efficiency of the configuration decreases more than proportionally with the cruising speed.

The actual channel wing of this study is not competitive at a reasonable Mach number range as the acceptable $\Delta Ma/Ma_\infty$ above the wing is comparatively small and drops to zero at Ma_∞ = 0.66.

It was, however, shown that, on the one hand, the position of the propeller and, on the other hand, the wing profile with its pressure distribution significantly affect the propulsive efficiency of the configuration. The general design rule is to minimize the local inflow velocity to the propeller whereas its position above the wing is mainly prescribed by aeroacoustic considerations. Note that the main advantage of an over-the-wing propeller is its noise shielding capability. In the best-case scenario, the possible improvements may reduce the efficiency loss to 5% at Ma_∞ = 0.6 which must be weighed against the advantages of a low-noise design. Nevertheless, it can be stated that channel wing configurations are restricted to Mach numbers below 0.6 and therefore not suited for commercial aircraft with more than 1000 km range.

Based on the results, future work will investigate the integration of a ducted propfan above the wing trailing edge to take advantage of the drag reduction effect at reduced inflow velocity to the rotor. Although the inlet distribution will be more homogeneous compared to the open rotor variant, inflow disturbances and their impact on fan aerodynamics and nacelle drag must be considered in detail.

6. ACKNOWLEDGEMENTS

This work was funded by the German Research Funding Organisation (DFG) in the framework of the collaborative research centre SFB 880. Computational resources have been gratefully provided by the North-German Supercomputing Alliance (HLRN). The authors would like to acknowledge Carsten Lenfers, DLR Braunschweig, Institute of Aerodynamics and Flow Technology (DLR-AS) for providing the propeller data and Jochen Wild (also DLR-AS) for providing the wing airfoil geometry. Further thanks go to Wolfgang Heinze of the Institute of Aircraft Design and Lightweight Structures, TU Braunschweig, for his multidisciplinary studies on the reference aircraft.

REFERENCES

[1] Airbus S.A.S., “Delivering the Future”, *Global Market Forecast 2011-2030*, Blagnac, France, 2011.

[2] C. Werner-Westphal, W. Heinze, P. Horst, “Multidisciplinary Integrated Preliminary Design Applied to Unconventional Aircraft Configurations,” *Journal of Aircraft*, Vol. 45, No. 2, 2008, pp. 581–590.

[3] L. Müller, W. Heinze, D. Kozulovic, M. Hepperle, R. Radespiel, “Aerodynamic Installation Effects of an Over-the-Wing Propeller on a High-Lift Configuration,” *Journal of Aircraft,* to be published 2013.

[4] L. Müller, M. Lummer, D. Kozulovic, J. Delfs, M. Hepperle, “Aerodynamic and Aeroacoustic Assessment of a High-Lift Channel Wing Configuration,” In: *SFB 880 - Fundamentals of high-lift for future commercial aircraft*, Biennial report. CFF Forschungsbericht 2013-03, Braunschweig, Germany, 2013.

[5] L. Müller, D. Kozulovic, M. Hepperle, R. Radespiel, “The Influence of the Propeller Position on the Aerodynamics of a Channel Wing,” In: *Proceedings of Deutscher Luft- und Raumfahrtkongress 2012*, Berlin, Germany, 2012.

[6] J.L. Johnson, E. White, “Exploratory Low-Speed Wind-Tunnel Investigation of Advanced Commuter Configurations Including an Over-the-Wing Propeller Design,” In: *Proceedings of the AIAA Aircraft Design, Systems and Technology Meeting*, Paper No. AIAA-83-2531, Fort Worth, TX (USA), 1983.

[7] L. Müller, D. Kozulovic, M. Hepperle, R. Radespiel, „Installation Effects of a Propeller Over a Wing with Internally Blown Flaps“, *Proceedings of the 30th AIAA Applied Aerodynamics Conference*, Paper No. AIAA 2012-3335, New Orleans, LA (USA) 2012.

[8] J. Wild, G. Wichmann, F. Haucke, I. Peltzer, and P. Scholz, “Large scale separation flow control experiments within the German Flow Control Network”, *Proceedings of the 47th AIAA Aerospace Sciences Meeting*, Paper No. AIAA 2009-0530, Orlando, FL (USA)

[9] C. Lenfers, “Propeller Design for a future QESTOL Aircraft in the BNF Project”, *Proceedings of the 30th AIAA Applied Aerodynamics Conference*, Paper AIAA 2012-3334, New Orleans, LA (USA) 2012.

[10] D. Schwamborn, T. Gerhold, R. Heinrich, “The DLR TAU-Code: Recent Applications in Research and Industry,” In: ECCOMAS CFD, Egmond aan Zee, The Netherlands, 2006.

[11] P.R. Spalart and S.R. Allmaras, “A One-Equation Turbulence Model for Aerodynamic Flows,” AIAA Paper, No. 92-0439, 1992.

[12] A. Raichle, S. Melber-Wilkening, and J. Himisch, “A New Actuator Disk Model for the TAU Code and Application to a Sailplane with a Folding Engine,” *Proceedings of the 15th STAB/DGLR Symposium*, Darmstadt, Germany, 2006.

[13] I. Kroo, “Propeller-wing integration for minimum induced loss,” *Journal of Aircraft*, Vol. 23, No. 7, pp. 561-565, 1986.

[14] D.P. Witkowski, A.K.H. Lee, J.P. Sullivan, “Aerodynamic Interaction Between Propellers and Wings,” *Journal of Aircraft*, Vol. 26, No. 9, pp. 829-836, 1989.